Eur. Phys. J. B **10**, 53–60 (1999)

THE EUROPEAN PHYSICAL JOURNAL B

EDP Sciences

Curvature walls and focal conic domains in a lyotropic lamellar phase

C. Blanc[a] and M. Kléman

Laboratoire de Minéralogie-Cristallographie de Paris[b], T16 case 115, 4 place Jussieu, 75252 Paris Cedex 05, France

Received 4 November 1998

Abstract. In the quasi-ternary CPCl/brine/hexanol lyotropic system, the interface of the L_α lamellar and L_3 sponge phases displays a phenomenon of epitaxy: the layers of the lamellar phase tend to make a constant non-trivial angle with the interface. Thin samples of lamellar phase embedded in the sponge phase are thus submitted to oblique anchoring conditions and defects are created in the lamellar phase in order to satisfy the bulk lamellar ordering and the boundary conditions. We have studied small droplets of lamellar phase in the sponge phase. They do not exhibit the classic L_α defects (focal conic domains) but wall defects, which appear in order to satisfy the smectic elasticity and the boundary conditions. Moreover we show through experiments in controlled geometry that, even in the presence of focal conic domains, wall defects control the size and periodicity of the textures which are observed at the interface.

PACS. 61.30.Jf Defects in liquid crystals – 68.10.Cr Surface energy (surface tension, interface tension, angle of contact, etc.)

1 Introduction

The L_3 sponge phase and the L_α lamellar phase both consist of membranes of surfactants in solvent. Whereas the membranes are stacked with smectic order in the L_α phase, the sponge phase is made of a disordered and multiply connected membrane which divides the solvent into two equivalent subvolumes [1–5]. The characteristic distances vary between a few tens of Å and 0.1 μm for the most dilute samples.

Previous studies of the cetylpyridinium chloride (CPCl)/hexanol/brine lyotropic system have shown that the interface between the L_3 and the L_α phases makes a constant non trivial angle θ_0 with the lamellar layers [6,7] (note however that deviations from this angle are observed when specific boundaries conditions are imposed: see Sect. 3). This effect is related to the continuity of the bilayers through the interface, which yields a matching of the characteristic distances d_α and d_3 of the two phases and a large anisotropy of the interface tension [8,9]. The most striking consequence of this epitaxy is the formation of complex and unusual shapes of lamellar droplets in sponge phase [6,7]. The present paper emphasizes the importance of the nature of the defects present in the droplets and the thin lamellar samples. A forthcoming article will provide a complete description of the nucleation and growth of these droplets.

The nucleation of a smectic phase in an isotropic one with specific boundary conditions is an old problem encountered for the first time by Friedel [10] when he studied the nucleation of SmA "bâtonnets". In this later case, the droplets are obtained during the SmA-isotropic phase transition and display numerous defects (in particular focal conic domains FCDs) which relax the surface energy by orienting the smectic layers perpendicular to the interface [11]. In the first part of this paper we shall find defects of an other type in the L_α bâtonnets (we shall keep this word to describe the lamellar droplets in the sponge phase). In particular we describe wall defects which have not been observed in the bâtonnet of the thermotropic SmA systems in which the FCDs are present down to the optical sizes [11,12].

In a second part we show that the wall defects are not confined to the bâtonnets but can combine with FCDs in order to satisfy imposed boundary conditions. We study in detail a geometry leading to the formation of focal conic lattices, whose geometrical parameters are controlled by the competition between wall defects, FCDs and interface energy.

2 Defects in the lamellar bâtonnets

2.1 Experiments

We have used the cetylpyridinium chloride (CPCl)/hexanol/brine system, in which a temperature transition occurs from the sponge phase to the lamellar phase [13].

[a] e-mail: blanc@lmcp.jussieu.fr
[b] UMR 7590

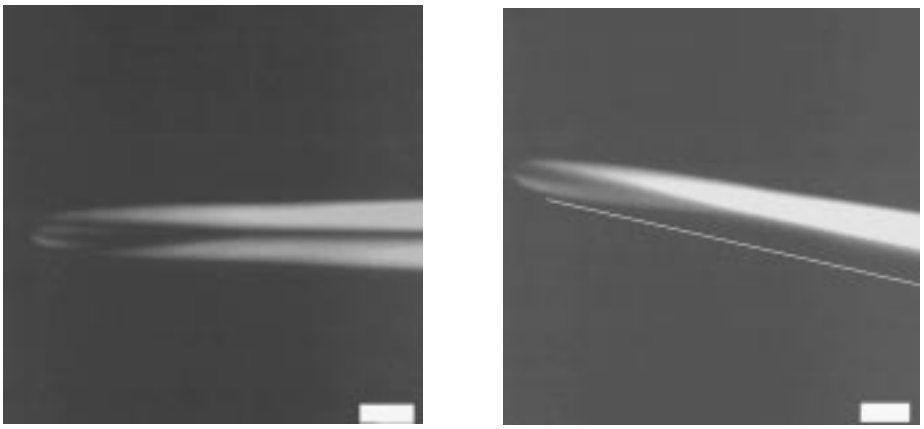

Fig. 1. Apex of elongated "Sword I" bâtonnet under crossed polarizers. The extinction of the birefrigent lamellar phase gives the geometry of the layers (vertical and horizontal polarizers; bar $\approx 20\,\mu$m)

Samples are prepared in the L_3 phase in the vicinity of the L_α-L_3 domain of coexistence at room temperature (brine 1%wt NaCl, wt ratio hexanol/CpCl = h/c = 1.113, mass fraction of the membrane 30%). The different components are mixed in test tubes for 30 min. Then the tubes are centrifuged for one hour and held a few days at rest. The solution is soaked into rectangular capillaries (Vitrodynamics microslides), the samples are sealed by flame and observed under an optical polarizing microscope (Leitz DMRXP) equipped with a hot stage (Mettler 82HT: temperature regulated at 0.1 °C), a movie camera and a movie-recorder.

Since the domain of coexistence is large (39 °C–83 °C for h/c = 1.113), stable lamellar droplets embedded in the sponge phase can be obtained by increasing the temperature. Their shapes strongly depend on growth conditions [7,9] but are stable during the duration of observation, after the bâtonnets have ceased growing (the droplets can be observed for approximately one hour). In this paper, we focus on elongated droplets (Fig. 1) of axial symmetry, resulting from a rapid growth (the velocity in the direction of the axis is $\approx 20\,\mu$m s^{-1}, which corresponds to an increase of ≈ 5 °C from 38 °C to 43 °C). The typical radius of the cylindrical part is smaller than $10 \sim 15\,\mu$m. Using the effect of birefringence between crossed polarizers, it appears that in most of the cylindrical bâtonnet, the lamellae stack along parallel cones (Fig. 2) whose boundaries satisfy the tilt contact $\theta_0 \approx 70°$ at the interface [7], while at the apex the layers adopt a geometry of concentric spheres, whose center is at the top of the bâtonnet. The two domains are separated by a surface on which the director is discontinuous at optical scale (Fig. 2).

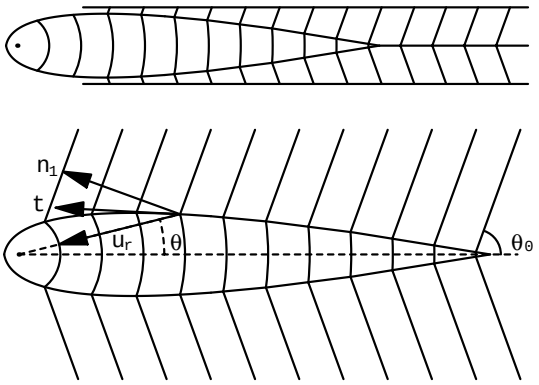

Fig. 2. Top: organization of the lamellae in the bâtonnet of Figure 1. Bottom: the tangent planes of the surface of discontinuity (SD) are the bisecting planes of the two lamellar organizations.

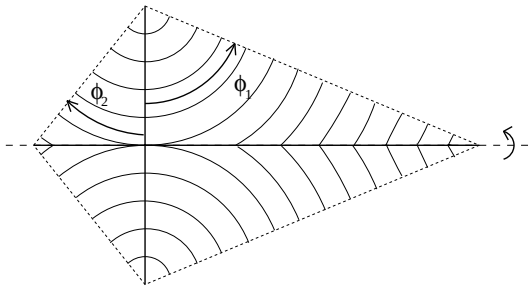

Fig. 3. Toric conic focal domain (TFCD). This particular FCD displays an ellipse and a straight line as lines of singularities.

2.2 Curvature walls

The usual macroscopic defects of the smectic materials are Focal Conic Domains (FCDs) (see Fig. 3). First described by Friedel [10], they correspond to lines defects and preserve the parallelism between the layers everywhere except along two lines of singularities: a set of conjugated ellipse and hyperbola. The FCDs assemble with well-defined rules [10,11,14–16]. In lyotropic systems, the focal conic can be of two types (first species and second species [17,18]) or reduced to points defects consisting of an assembly of spherical layers (spherolites). The smectic bâtonnets have been described as a complex assembly of FCDs with some point defects [10,11,19].

However, other types of defects are documented, like wall defects, *e.g.* in SmC samples the *chevron* texture (see Ref. [20] and references therein: experiments of X-ray scattering and optical observations), in some SmA

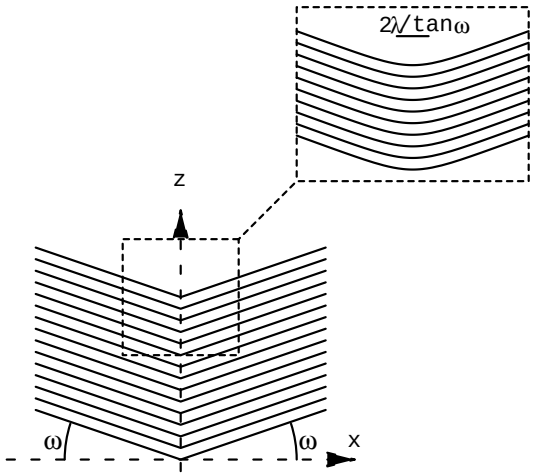

Fig. 4. Curvature wall at optical and interlamellar scale.

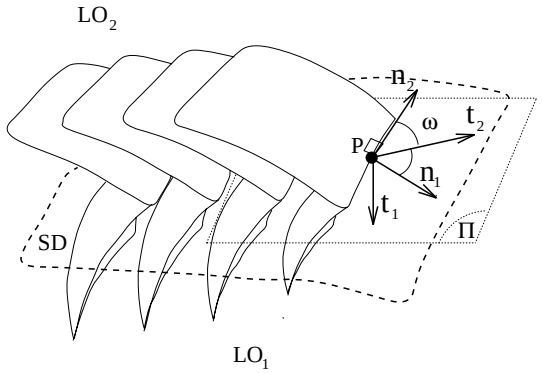

Fig. 5. Curvature wall at optical scale between two different lamellar organizations.

samples (*chevron* texture) in the vicinity of the SmA-SmC transition [21,22] and in lamellar diblock copolymers: *tilt boundaries* observed by transmission electron microscopy [23] and numerically simulated [24]. Various models, based on Landau-De Gennes theories, have been developed in references [20,25,26] (SmC) and [27] (SmA).

Curvature walls (or small angle discontinuity walls), which have been theoretically studied [28–30] have never been reported in the SmA thermotropic bâtonnets. Their observations in L_α growth nuclei and bulk samples are the first to have ever been made in a lyotropic phase.

We use the results of a simplified model which successfully explain the observations. The basic geometry is as in Figure 4: far from the z-axis the normal of the layers is rotated by an angle ω. The total energy splits in a curvature part and a compression part:

$$\mathcal{E}_w = \iiint \frac{K}{2}\left(c_1 + c_2\right)^2 + \frac{\bar{B}}{2}\left(1 - \frac{d}{d_0}\right)^2 \mathrm{d}\tau. \qquad (1)$$

$K = \kappa/d_0$ is the curvature modulus (κ is the curvature modulus for one layer), $\bar{B}$ the compression modulus, c_1 and c_2 the principal radii of curvature (here $c_2 = 0$), d the local interlamellar thickness, d_0 the interlamellar thickness without compression. In the small angle limit $\omega \ll 1$ ($c_1 \approx \mathrm{d}\theta/\mathrm{d}x$ and $(1 - d/d_0) \approx (\omega^2 - \theta^2)/2$, where θ is the local angle of the layer with the plane $z = 0$), the energy by unit length of wall is [28]:

$$\mathcal{E}_w = \frac{2K}{3\lambda}\omega^3 \qquad (2)$$

where λ is the smectic penetration length ($\lambda = \sqrt{K/\bar{B}}$ compares with d_0). We present in Appendix A the solution valid for larger angles. The width of the wall is given by $s \approx 2\lambda/\tan\omega$, which is a microscopic length (with typical values $\lambda \approx d \approx 10^{-8}$m and $\omega \approx 10°$, $s \approx 0.1\,\mu$m). Thus a curvature wall appears as an angle-discontinuity wall at optical scale, but at microscopic scale its major feature is the continuity of the layers.

2.3 Curvature walls at optical scale

If no special experimental precautions are taken to align the sample, the radii of curvature of the lamellar layers are of the order of the thickness of the sample (or of the size of the droplet). Thus wall defects are not expected to be plane on a large scale (as in Fig. 4) but rather to take the shape of curved surfaces of discontinuity (SDs) between different lamellar organizations. In this section we discuss the conditions of existence of such surfaces and establish their equation.

Let $\mathbf{n}_1(\mathbf{P})$ and $\mathbf{n}_2(\mathbf{P})$ be the respective directors fields of two lamellar organizations $LO1$ and $LO2$ (see Fig. 5). Locally the surface SD between the lamellar organizations is described by a plane curvature wall if the macroscopic radii of curvature are much larger than the width of the walls, which is usually the case. Moreover SD has to satisfy the continuity of the layers, thus locally its tangent plane $\mathit{\Pi}(\mathbf{P})$ is the bisecting plane of the two stackings. $\mathit{\Pi}(\mathbf{P})$ is then defined by the tangent vectors $\mathbf{t}_1(\mathbf{P}) = \mathbf{n}_1(\mathbf{P}) \times \mathbf{n}_2(\mathbf{P})$ and $\mathbf{t}_2(\mathbf{P}) = \mathbf{n}_1(\mathbf{P}) + \mathbf{n}_2(\mathbf{P})$ or by a normal vector $\mathbf{t}_3(\mathbf{P}) = \mathbf{n}_1(\mathbf{P}) - \mathbf{n}_2(\mathbf{P})$. The surfaces SDs exist if and only if the vector field $\mathbf{t}_3(\mathbf{P})$ verifies the condition of integrability:

$$\mathbf{t}_3.\nabla \times \mathbf{t}_3 = \mathbf{0}. \qquad (3)$$

Since LOi ($i = 1$ or 2) is a geometric smectic organization, its layers form a set of parallel surfaces, hence $\nabla \times \mathbf{n}_i = \mathbf{0}$ (this approximation excludes layers dilation or compression in the bulk). Equation (3) is verified and SD can be constructed by solving:

$$\begin{cases} \dfrac{\partial \mathbf{P}}{\partial u} = \mathbf{t}_1(\mathbf{P}) \\ \dfrac{\partial \mathbf{P}}{\partial v} = \mathbf{t}_2(\mathbf{P}) \end{cases} \qquad (4)$$

where (u, v) are local coordinates of the surface SD. Note that, since the vector fields $\mathbf{n}_i$ derive from potentials φ_i, $\mathbf{t}_3 = \nabla(\varphi_1 - \varphi_2)$ and the surfaces SD are given by $\varphi = \varphi_1 - \varphi_2 = \text{const}$. In general $\nabla \times (\mathbf{t}_3/\|\mathbf{t}_3\|) \neq \mathbf{0}$ thus the set of surfaces SDs are not parallel.

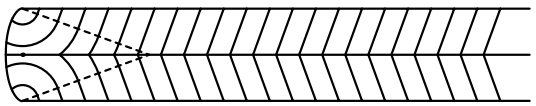

Fig. 6. A FCD ending the bâtonnet is observed in large droplets.

The smectic energy of such a wall is thus given by:

$$\mathcal{E}_w = \frac{2K}{3\lambda} \iint_w \omega^3 \mathrm{d}S \tag{5}$$

where $2\omega \approx \|\boldsymbol{\nabla}\varphi_1 \times \boldsymbol{\nabla}\varphi_2\|$.

Let us apply those considerations to our experimental case: we have sketched in Figure 2 the normal of the layers of the spherical and the conical stackings in a plane containing the axis of the droplet. The trace of the surface in this plane is then the bisecting line of the directors. We use polar coordinates and the origin is the center of the spherical stack. The normal of the conical layers is $\mathbf{n}_1 = -\cos(\theta+\eta)\mathbf{u}_r + \sin(\theta+\eta)\mathbf{u}_\theta$ where η is $\frac{\pi}{2} - \theta_0 \approx 20°$ ($\mathbf{n}_1 = \boldsymbol{\nabla}\varphi_1$ with $\varphi_1 = -r\cos(\theta+\eta)$) and the normal of the spherical layers is $\mathbf{n}_2 = -\mathbf{u}_r$ ($\varphi_2 = -r$), thus a tangent vector of the wall is:

$$\mathbf{t} = -\left(\cos(\theta+\eta)+1\right)\mathbf{u}_r + \sin(\theta+\eta)\mathbf{u}_\theta. \tag{6}$$

The equations of the walls $r(\theta)$ are thus given by:

$$\frac{1}{r}\frac{\mathrm{d}r}{\mathrm{d}\theta} = -\frac{\cos(\theta+\eta)+1}{\sin(\theta+\eta)} = -\frac{1}{\tan\left(\frac{\theta+\eta}{2}\right)} \tag{7}$$

$$r(\theta) = \frac{r_0}{\sin^2\left(\frac{\theta+\eta}{2}\right)} \tag{8}$$

which are the equipotential surfaces of $\varphi = r - r\cos(\theta+\eta)$. This analytical surface matches quite closely the surface discontinuity SD we have observed (shape and angle). The greater section $r_0/\sin\eta$ is close to the radius of the bâtonnet and gives the value of r_0.

2.4 Competition with focal conic domains

Wall defects are not observed in SmA materials (except in the few cases reported above as chevron texture) since a small angle grain boundary is unstable and tends to collapse into a set of focal conics [15,30]. In our system, the observations show that the more complex droplets display focal conic domains when their size is typically larger than $20 \sim 30\,\mu$m, but the smaller ones display only curvature walls. This behavior results from a competition between the elastic energies of the defects. The defects relax the interface energy (more precisely its anisotropic part [19]) which varies as $\Delta\sigma r^2$ where $\Delta\sigma$ is a typical value of the anisotropy of surface tension and r a typical size of the droplet. The energy of a curvature defect varies as $K\omega^3 r^2/\lambda$ and a focal conic domain as Kr. Thus the focal conic domains appear when the typical size of the droplet is larger than $r \approx \lambda/\omega^3$. For example an alternative to the surface SD in the studied droplet is the nucleation of a focal conic domain at the apex (see Fig. 6) (a similar defect is experimentally observed for some larger bâtonnets). A comparison between the two defects is given in Appendix B and yields a critical size $r \approx 10\,\mu$m which has the good order of magnitude.

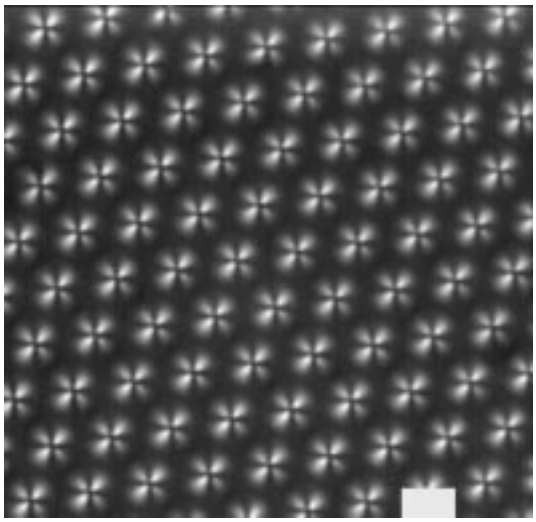

Fig. 7. Hexagonal lattice of focal conic between crossed polarizers. Bar = $20\,\mu$m (thickness of the slab $\approx 60\,\mu$m).

In conclusion, this part completes the previous works on the different studies of bâtonnets. The hierarchy of defects inside a bâtonnet is the following: below optical scale (but above a critical size of nucleation) the droplets are supposed to display flat layers and the ideal shape given by the classic Wulff construction [11]. In larger bâtonnets, the interface energy is relaxed by the creation of wall defects and point defects, and above a critical size r (in the present system $r \approx 20 \sim 30\,\mu$m) focal conic domains appear.

3 FCDs and walls

We have insisted on the competition between the FCDs and the walls in the bâtonnets. In fact, those defects can be found in the presence of FCDs but they are often much less visible. Their presence is nevertheless necessary to create the various structures encountered in the $L_\alpha - L_3$ domain of coexistence.

3.1 Experiments

The local interaction of the lamellar phase is steric [35] and the lamellae near the glass of the capillary are aligned by the presence of the wall. If the growth is slow enough (typically $< 0.1\,°\mathrm{C\ min}^{-1}$), the lamellar phase grows from the wall, with tangential orientation at the interface and consequently with an unfavourable interface energy. As soon as the thickness of the sample is large enough, an hexagonal lattice of defects appears (Figs. 7 and 8).

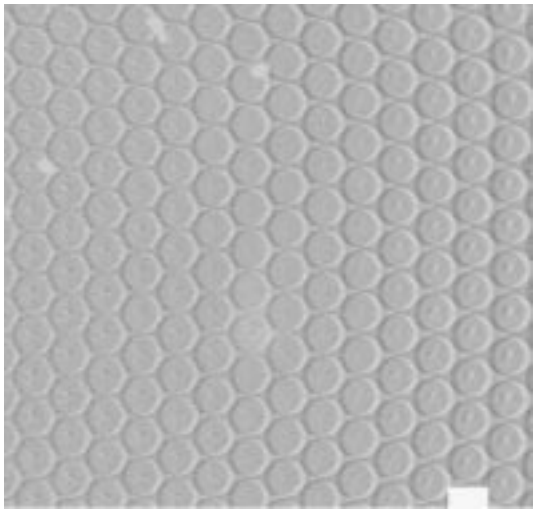

Fig. 8. Hexagonal lattice of focal conic domains in parallel light. Bar = 20 μm (thickness of the slab $\approx$ 60 μm).

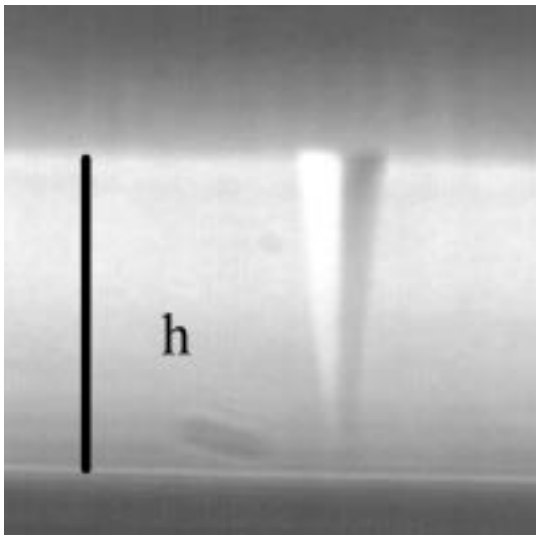

Fig. 9. View of the defect on the side boundary of the capillary. The defect is embedded in an homeotropic stacking. $h \approx 37\,\mu$m.

Similar lattices have also been observed in SmA liquid crystals [10,31,32] and already reported in our system [6]. We study in detail the present lattice and show up that it requires the presence of walls coupled to FCDs on macroscopic scales.

Hexagonal lattices have been usually described as sets of toric focal domains TFCDs which relax the surface energy (see different geometric models in [31,33]). We have studied the nucleation of those objects in rectangular capillaries 4 000 μm $\times$ 300 μm. On the lateral wall of the capillary, as long as the slab of lamellar phase is thin enough, no defects are visible although the contact between the lamellar phase and the sponge phase is tangential and thus energetically unfavourable. After the thickness has reached 35$-$40 μm, isolated defects appear (Fig. 9). One can see on the lateral side of the capillary a focal conic domain embedded in the stacking of flat lamellar layers. The

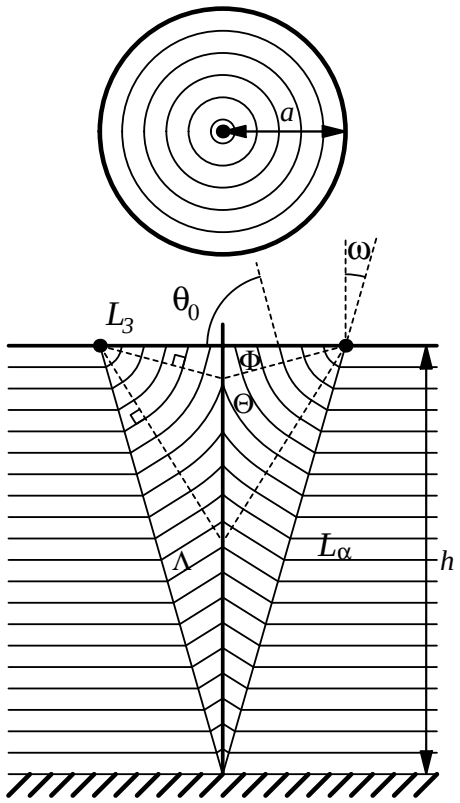

Fig. 10. Simplest construction of an isolated defect which fulfils the optical observations and the boundary conditions (view from above and side view).

study of the birefringence indicates that the outer surface of the defect is an angle-discontinuity wall.

It must be noticed that the nucleation of the defects, contrary to the case described by [31], is quite independent from the growth conditions. Even at low velocities ($< 0.1\,\mu$m min^{-1}), the nucleation of isolated defects begins at $h \approx 35{-}40\,\mu$m at the studied dilution. When the temperature is decreased, the lattice disappears at the same thickness. Moreover, when destroyed (temperature jump or mechanical constraint on the substrate), the lattice reconstitutes in a few minutes. It is therefore probable that the energy barrier corresponding to the nucleation of the defects is rather low and we will neglect the dynamical processes in the following model.

3.2 Geometry of the model

The simplest geometry, which satisfies the following conditions and the optical observations is given (Fig. 10) in a plane containing the z-axis: the angle-discontinuity walls are symmetric (continuity of the layers), the contact angle at the interface is θ_0 at the part of interface which is inside the conical region Φ, and the contact between the layers and the capillary is everywhere tangential except at one point. A conical symmetric wall separates the flat layers and the defect. From the surface of the defect, one finds a conical stack, then a part of a focal domain and finally

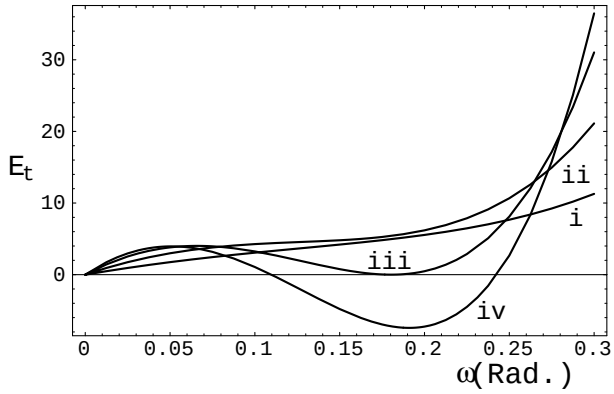

Fig. 11. Total energy of one isolated defect as a function of the angle ω. The different curves correspond to (i) $x = 40$, (ii) $x = 80$, (iii) $x = 128$, (iv) $x = 160$. A defect appears when $E_t = 0$, the critical thickness $x = 128$ compared with the experimental value $h = 37 \pm 2\,\mu$m gives $\alpha\lambda \approx 3 \times 10^{-7}$m.

a second conical stack, which matches the flat interface at the contact angle θ_0. The dashed lines represent walls on which the directions of the normal vary continuously, but where the curvatures are discontinuous (called second order walls [34]).

3.3 Energetics

The study of the major features of these structures will be divided in two stages. First we analyze the nucleation of individual defects. Then we study the lattices, in which the objects are not isolated.

Let $\Delta\sigma$ be the positive difference between the tangential surface energy and the tilt angle surface energy, thus the gain in interface energy is given by:

$$\begin{aligned} \mathcal{E}_s &= -\Delta\sigma\pi a^2 = -\Delta\sigma\pi h^2 \tan^2\omega \\ \mathcal{E}_s &\approx -\Delta\sigma\pi h^2\omega^2 \end{aligned} \tag{9}$$

where 2ω is the angular discontinuity at the wall, h the thickness of the lamellar phase and a the radius of the circle. The lamellae are parallel everywhere in the defect except on the surfaces and lines of discontinuity, and the compression can be neglected (this classic approximation is valid when the radii of curvature are larger than λ). We follow [12,31] for the computation of the smectic energy $\mathcal{E}_{fc}$ inside the cone. The focal domain energy is constituted by a term of curvature and a term of defect along the axis. As the angle ω remains small we can consider that the curvature energy is the same than a semi-infinite focal domain and is given by $\alpha\pi Ka$ with $\alpha \approx 20 \sim 30$ (see Appendix C). Thus:

$$\mathcal{E}_{fc} = \alpha\pi Kh\tan\omega \approx \alpha\pi Kh\omega. \tag{10}$$

The angle discontinuity 2ω is constant on the wall of area $\pi a^2/\sin\omega$, thus its energy is given by:

$$\mathcal{E}_w \approx \frac{2K\pi h^2}{3\lambda}\omega^4. \tag{11}$$

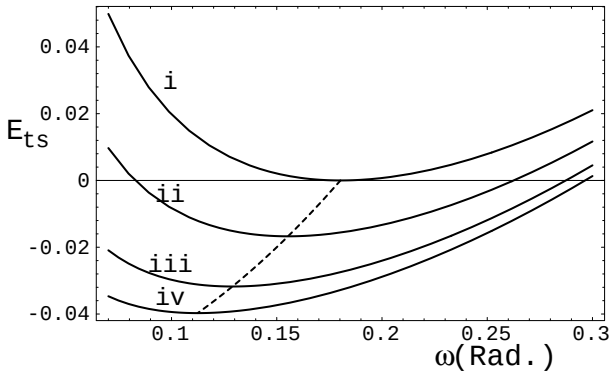

Fig. 12. Total energy of the lattice by unit of area. The different curves correspond to a thickness (i) $x = 128$, (ii) $x = 200$, (iii) $x = 350$, (iv) $x = 528$.

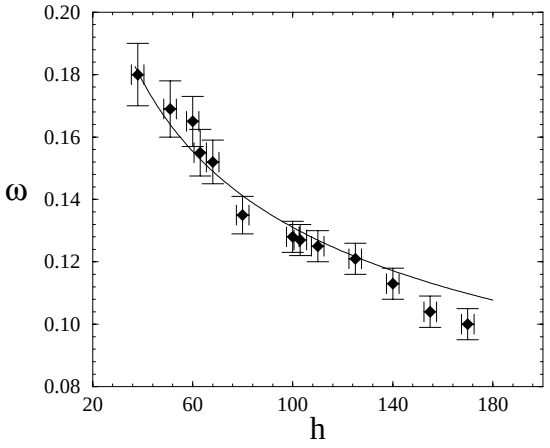

Fig. 13. Evolution of ω (rad.) *vs.* the thickness h (μm) of the lamellar phase.

The dimensionless energy $E_t = (\mathcal{E}_s + \mathcal{E}_w + \mathcal{E}_{fc})/K\alpha^2\lambda\pi$ represents the energy of the total defect and is given by:

$$E_t = -\Phi x^2\omega^2 + x\omega + 2x^2\omega^4/3 \tag{12}$$

where $\Phi = \Delta\sigma\lambda/K$ and $x = h/\alpha\lambda$. For small x, E_t takes positive values, no defect is present. Then the minimum of E_t reaches zero and the defect appears, its geometry is defined by the angle $\omega = \sqrt{\Phi/2}$, corresponding to the minimum of E_t. Experiments give $\omega = 0.18 \pm 0.01$ rad, which means that $\Phi \approx 0.065$, which is in the range of expected values (a value $\Phi \approx 0.07$ is obtained from $\Delta\sigma \approx \sigma/10$ with $\sigma \approx \kappa/d_3^2$ (see [8]) and $d_3 \approx 1.2d_\alpha$ [6]). The critical thickness $h \approx 35 \sim 40\,\mu$m gives the product $\alpha\lambda = 3 \times 10^{-7}$ m which is satisfactory since $\alpha \approx 20 \sim 30$ (see Appendix C) and $\lambda \approx d \approx 10^{-8}$ m. Several plots are given in Figure 11, they correspond to the value $\alpha\lambda = 30 \times 10^{-8}$ m, $\Phi = 0.065$.

When the thickness of the lamellar slab increases, the lattice forms rapidly. Beyond h_c, the size of the defects inside the lattice is no longer given by the minima of the previous curves (a slight increase of the tilt angle ω towards a stationary value $\omega = \sqrt{3\Phi/4} \approx 0.22$ is expected).

The measurements show on the contrary a rapid decrease of the angle ω (see Fig. 13). Since a defect is not isolated in the lattice but is in contact with its closest neighbors (see Fig. 8), the previous analysis has to be modified. The geometry of one defect in the lattice is assumed to be the same (as the optical observations in the lateral geometry strongly suggest it), but the minimization has now to be performed at constant total area of the interface, *i.e.* it is the energy by unit of area which has to be minimized:

$$E_s \propto E_{ts} = E_t/x^2\omega^2 = -\Phi + 1/x\omega + 2\omega^2/3. \qquad (13)$$

Different curves $E_{ts}(\omega)$ are given in Figure 12 for different values of x. The local minimum has been reported in the Figure 13 (its equation is $\omega = (3/4x)^{1/3}$). It fits the decrease of ω with the previous value $\alpha\lambda = 30 \times 10^{-8}$ m. Note however the slight discrepancy due either to terms neglected or more probably to the expression of the energy of the wall, which has been obtained in the framework of a simple model.

4 Conclusion

To summarize, in a first part we have shown that wall defects were necessary to explain the smectic organization in lamellar droplets, especially in small droplets where focal conics are not present. We have given rules to construct geometrically a wall separating two different known regions. In a second part we have shown how wall defects are combined with focal conic to relax surface energy and satisfy boundaries conditions at the same time. The comparison between experiments and theory is quite good even with the rough approximations at work. We can thus conclude that the elastic model we have used is a good approximation for the energy of the wall defect. We think that angle-discontinuity walls are important to explain the optical observations each time there exists a visible low limit to the size of the FCDs (regular textures, oily streaks, isolated focal conic domains, textures appearing under shear). Although they are much less visible than FCDs, angle discontinuity walls seem to play an important role in the lamellar macroscopic behavior. We have illustrated this fact by the study of the focal conic lattice where the energy of the wall defects rules the sizes of the lattice.

Appendix A: Curvature walls: an extension to larger angles

We refer here to Figure 4. Let s be the curvilinear abscissa along a layer and θ the local angle of the layer with the plane $z = 0$ (θ varies between $-\omega$ and ω), the radius of curvature and the interlamellar distance are then given by [36]:

$$\begin{aligned} c_1 &= \frac{\partial\theta}{\partial s} \\ d &= d_0 \frac{\cos\theta}{\cos\omega}. \end{aligned} \qquad (A.1)$$

In the case of layers of surfactants embedded in solvent, the elastic energy energy corresponding to a layer is by unit of length:

$$\mathcal{E}_{la} = \int_{-\infty}^{+\infty} \frac{\kappa}{2}\left(\frac{\partial\theta}{\partial s}\right)^2 + \frac{\bar{B}d_0}{2}\left(1 - \frac{\cos\theta}{\cos\omega}\right)^2 \mathrm{d}s. \qquad (A.2)$$

The minimization can be exactly solved and we obtain:

$$\theta(s) = 2\arctan\left(\tan(\frac{\omega}{2})\tanh\left(\frac{\tan\omega s}{2\lambda}\right)\right). \qquad (A.3)$$

This expression becomes $\theta(s) = \omega\tanh(\omega x/2\lambda)$, when $\omega \ll 1$ and $s \approx x$. The total energy by unit of length for each layer is thus given by:

$$\mathcal{E}_{la} = \frac{2\kappa}{\lambda}(\tan\omega - \omega). \qquad (A.4)$$

Since $\cos\omega/d_0$ layers by unit of length cross the wall, the total energy of the wall, by unit of area, is:

$$\mathcal{E}_w = \frac{2K}{\lambda}(\tan\omega - \omega)\cos\omega \qquad (A.5)$$

which simplifies in $\mathcal{E}_\omega \approx \frac{2K\omega^3}{3\lambda}$ when $\omega \ll 1$.

Appendix B

In this Appendix, we compare the energies of the bâtonnet of Figure 2, which ends with a curvature wall defect and the bâtonnet sketched in Figure 6, which ends with a FCD domain. The general expression which gives the energy of a toric focal conic domain (see Fig. 3) is [16]:

$$\begin{aligned} \mathcal{E}_{fc} = {} & 2\pi Ka\left[\ln\frac{a}{r_c} - 2 - \frac{\bar{K}}{K}\right](\phi_1 - \phi_2) \\ & - 2\pi Ka\int_{\phi_1}^{\phi_2} \ln(\cos\phi)\mathrm{d}\phi \end{aligned} \qquad (B.1)$$

where ϕ_1 and ϕ_2 are the angle of the cone boundaries, r_c a core radius (typically $r_c \approx d \approx 10^{-8}$ m), K the curvature modulus and a the radius of the circle. When the singularity energy along the hyperbola (the revolution axis here) is taken into account, we obtain a total energy $\alpha K\pi a$ with $\phi_1 = 0$, $\phi_2 = \pi/2$ and $\alpha = 20 \sim 30$ (see Appendix C).

The energy of the wall defect is given by:

$$\mathcal{E}_w = \frac{2K}{3\lambda}\int_0^{\theta=\eta}\left(\frac{\eta+\theta}{2}\right)^3 \mathrm{d}S \qquad (B.2)$$

(the upper boundary corresponds to the maximum lateral size of the spherical stacking). With $\eta \ll 1$, one gets:

$$\mathcal{E}_w = \frac{16\pi Ka^2\eta^2}{3\lambda}\left(\ln 2 - \frac{1}{2}\right) \approx \frac{3Ka^2\eta^2}{\lambda} \qquad (B.3)$$

where a is the radius of the cylinder part. The comparison of the two terms gives a critical radius $a \approx \alpha\lambda\pi/3\eta^2$, above which the FCD is stable. Using the experimental value $\alpha\lambda = 30 \times 10^{-8}$m (see Sect. 3), $a \approx 2.5\,\mu$m which has the good order of magnitude ($a_{\exp} \approx 10 \sim 15\,\mu$m).

Appendix C

In this Appendix, the smectic energy of the defect in Figure 10 is estimated. We distinguish three different regions (labeled Λ, Θ and Φ). In Λ, the layers form a cone and their curvature energy is given by (using the approximation of small angle ω):

$$\mathcal{E}_\Lambda \approx 2K\pi\omega^2 h\left(\ln\frac{a}{r_c}-1\right) \tag{C.1}$$

where a is the radius of the circle. In the same way, the curvature energy in Φ is:

$$\mathcal{E}_\Phi \approx K\pi\omega\eta h\left(\ln\frac{a}{r_c}-1\right). \tag{C.2}$$

The region Θ is a part of a toric focal domain and its curvature energy is given by [16,37]:

$$\mathcal{E}_\Theta = 2\pi Ka\left[\ln\frac{a}{r_c}-2-\frac{\bar{K}}{K}\right]\left(\frac{\pi}{2}-2\omega-\eta\right) - 2\pi Ka\int_\eta^{\pi/2-2\omega}\ln(\cos\phi)\mathrm{d}\phi \tag{C.3}$$

with the approximation $\omega \ll 1$ and $\eta \ll 1$, at the first order in ω:

$$\mathcal{E}_\Theta = \pi^2 Kh\omega\left[\ln\frac{2a}{r_c}-2-\frac{\bar{K}}{K}\right]. \tag{C.4}$$

Note that the core energies along the lines of defects are not taken into account in this curvature energy. In this regions of small extent, the compression energy is important. We assume that along the circle, the first lamellae is located at a distance r_c, thus no other contribution is needed. Along the hyperbolae degenerate into a straight line L, the situation is more complex (see Ref. [38]). In an elastic model, the line defect can be seen as a degenerated wall defect. Thus the local energy depends of the angle of the lamellae with the line (see the solution in SmA far from the ellipse in Ref. [39]). For a "semi-infinite toric domain" ($\phi_1 = 0$ and $\phi_2 = \pi/2$):

$$\mathcal{E}_h = \int_L \mathcal{E}_l(\theta)\mathrm{d}l = a\int_0^{\pi/2}\frac{\mathcal{E}_l(\theta)}{\sin^2\theta}\mathrm{d}\theta. \tag{C.5}$$

Thus we get a supplementary term in $h\omega$, which can be incorporated in $\mathcal{E}_\Theta$. Comparing the different terms, in first order in ω, the total smectic energy in the defect can be written as:

$$\mathcal{E}_{fc} \approx \mathcal{E}_\Theta = \alpha\pi Kh\omega. \tag{C.6}$$

The experimental value $\alpha\lambda = 3\times10^{-7}$ m obtained in Section 3, provides an estimation of $\alpha \approx 30$ with $\lambda \approx d_0 \approx 10^{-8}$ m. Since $\bar{K}/K$ is expected to be positive but low in the vicinity of the lamellar-to-sponge transition, this value compares with the order of magnitude given by $\pi(\ln(2a/r_c)-2) \approx 18$, where $a = 10\,\mu$m, $r_c = 10^{-8}$ m.

References

1. G. Porte, J. Marignan, P. Bassereau, R. May, J. Phys. France **49**, 511 (1988).
2. D. Anderson *et al.*, J. Phys. Chem. **93**, 4243 (1988).
3. D. Gazeau *et al.*, Europhys. Lett. **9**, 447 (1989).
4. D. Roux *et al.*, Europhys. Lett. **11**, 229 (1990).
5. D. Filali *et al.*, J. Phys. II France **4**, 349 (1994).
6. C. Quilliet, C. Blanc, M. Kléman, Phys. Rev. Lett. **77**, 522 (1996).
7. C. Quilliet *et al.*, C.R. Acad. Sci. Paris Ser. II **319**, 1469 (1994).
8. O.D. Lavrentovich, C. Quilliet, M. Kléman, J. Phys. Chem. B **101**, 420 (1997).
9. C. Blanc, M. Kléman (to be published).
10. G. Friedel, Ann. Phys. (Paris) **18**, 273 (1922).
11. J.-B. Fournier, G. Durand, J. Phys. II France **1**, 845 (1991).
12. J.-B. Fournier, Ph.D. thesis, University of Paris Sud, France, 1991.
13. Y. Nastishin, E. Lambert, P. Boltenhagen, C.R. Acad. Sci. Paris Ser. IIb **321**, 205 (1995).
14. Y. Bouligand, J. Phys. France **33**, 525 (1972).
15. M. Kléman, Rep. Prog. Phys. **52**, 555 (1989).
16. P. Boltenhagen, M. Kléman, O.D. Lavrentovich, *Focal conics domains in smectics, in Soft Order in Physical Systems,* edited by Y. Rabin, R. Bruinsma (1994), p. 5.
17. P. Boltenhagen, M. Kléman, O.D. Lavrentovich, C.R. Acad. Sci. Ser. II **52**, 931 (1992).
18. P. Boltenhagen, O.D. Lavrentovich, M. Kléman, Phys. Rev. A **46**, R1743 (1992).
19. O.D. Lavrentovich, Sov. Phys. JETP **64**, 984 (1986).
20. N. Vaupotič, M. Čopič, T.J. Sluckin, Phys. Rev. E **57**, 5651 (1998).
21. Y. Takanishi *et al.*, Jap. J. Appl. Phys. **28**, L487 (1989).
22. Y. Ouchi *et al.*, Jap. J. Appl. Phys. **28**, 2547 (1989).
23. S.P. Gido, E.L. Thomas, Macromolec. **27**, 6137 (1994).
24. R.R. Netz, D. Andelman, M. Schick, Phys. Rev. Lett. **79**, 1058 (1997).
25. N. Vaupotič *et al.*, Phys. Rev. E **54**, 3783 (1996).
26. L. Limat, Europhys. Lett. **44**, 205 (1998).
27. L. Limat, J. Prost, Liq. Cryst. **13**, 101 (1993).
28. P.-G. De Gennes, *The Physics of Liquid Crystals* (Oxford Clarendon, 1993).
29. M. Kléman, *Points, lignes, parois* (les Éditions de Physique, Orsay, 1977).
30. R. Bidaux *et al.*, J. Phys. France **34**, 661 (1973).
31. J.-B. Fournier, I. Dozov, G. Durand, Phys. Rev. A **41**, 2252 (1990).
32. M. Steers, M. Kléman, C. Williams, J. Phys. Lett. **35**, L21 (1974).
33. O.D. Lavrentovich, M. Kléman, V.M. Pergamenshchick, J. Phys. II France **4**, 377 (1994).
34. Y. Bouligand, J. Phys. France **41**, 1297 (1980).
35. W. Helfrich, Z. Naturforsch. A **33**, 305 (1978).
36. P. Oswald, Ph.D. thesis, University of Paris Sud, France (1981).
37. M. Kléman, J. Phys. France **38**, 1511 (1977).
38. J.-B. Fournier, Phys. Rev. E **50**, 2868 (1994).
39. P.-G. de Gennes, C.R. Acad. Sci. Paris Ser. B **275**, 549 (1972).